Polym. Korea, Vol. 50, No. 3, pp. 431-443 (2026)
https://doi.org/10.7317/pk.2026.50.3.431
ISSN 2234-8077(Online)

이핵 티타늄 FI 촉매 유래 다이아몬드 함유 이중모드 폴리에틸렌 복합재료를 이용한 해저 케이블 절연 연구

Ying Deng, Chunmeng Jiang, Luopeng Huang, Aimin Pan*,†, and Lesly Dasilva Wandji Djouonkep**,***,†

School of Electrical and Electronic Engineering, Wuhan Institute of Shipbuilding Technology
*School of Electronics and Information Engineering, Wuhan Donghu University
**Department of Petroleum Engineering and Applied Chemistry, Yangtze University
***Institute of Fine Organic Chemicals & Organic Materials, School of Chemistry and Chemical Engineering, Wuhan University of Science and Technology

(2025년 11월 6일 접수, 2026년 1월 26일 수정, 2026년 1월 27일 채택)

Diamond-Filled Bimodal Polyethylene Composites Derived from Binuclear Titanium FI Catalyst for Marine Cable Insulation

Ying Deng, Chunmeng Jiang, Luopeng Huang, Aimin Pan*,†, and Lesly Dasilva Wandji Djouonkep,***,†**

School of Electrical and Electronic Engineering, Wuhan Institute of Shipbuilding Technology, Wuhan 430050, China
**School of Electronics and Information Engineering, Wuhan Donghu University, Wuhan 430212, China;*
***Department of Petroleum Engineering and Applied Chemistry, Yangtze University, Wuhan 430100, China*
****Institute of Fine Organic Chemicals & Organic Materials, School of Chemistry and Chemical Engineering, Wuhan University of Science and Technology, Wuhan 430081, China*

(Received November 6, 2025; Revised January 26, 2026; Accepted January 27, 2026)

Abstract: A novel binuclear titanium FI catalyst bearing bulky tert-butyl substituents was synthesized from a bisphenol A backbone and applied to ethylene polymerization. When activated with methylaluminoxane (MAO), the catalyst exhibited extremely high activity of 9.8×10^6 g PE mol^{-1} Ti h^{-1}, producing genuinely bimodal high-density polyethylene with a weight-average molecular weight of 4.8×10^5 g mol^{-1}, a polydispersity index of 2.5, and a melting point of 134.2 °C. Composite films (18–40 μm thick) were prepared by melt-compounding the bimodal polyethylene with 10 parts by mass of diamond micropowders (average particle size 1.75–3.75 μm) followed by blown-film extrusion. The resulting diamond-filled composites displayed outstanding dielectric performance (breakdown strength 285–312 kV mm^{-1}, dielectric constant 2.68–2.86 at 1 kHz), high in-plane thermal conductivity (6.1–6.6 $Wm^{-1}K^{-1}$), and excellent dimensional stability (thermal shrinkage ≤ 0.42% at 150 °C). These properties surpass those of commercial biaxially oriented polypropylene (BOPP) capacitor films and meet the stringent requirements for next-generation marine power-cable insulation and high-voltage capacitor films. This work highlights the unique combination of a rigid bisphenol-A-bridged binuclear FI catalyst and diamond-filled bimodal polyethylene, providing a new route to advanced insulating materials for demanding electrical applications.

Keywords: binuclear FI catalyst, bimodal polyethylene, diamond-filled composites, dielectric/thermal conductive films, marine cable insulation.

Introduction

Marine power cables and high-voltage capacitor films require insulating materials that combine exceptional dielectric strength, thermal conductivity, dimensional stability under heat, and resistance to harsh environments. Conventional biaxially oriented polypropylene (BOPP) films, despite widespread use in capacitors, suffer from relatively low thermal conductivity (~0.24 W $m^{-1}K^{-1}$) and significant thermal shrinkage (>1.8% at 150 °C), limiting their performance in next-generation high-power-density systems.[1,2] Polyethylene-based materials, particularly bimodal high-density polyethylene (HDPE), offer superior mechanical toughness, environmental stress-cracking resistance, and processability, making them attractive alternatives if dielectric and

†To whom correspondence should be addressed.
panaimin2025@163.com, ORCID 0009-0003-3363-3250
dasilvawdl@outlook.com, ORCID 0000-0002-8190-5391

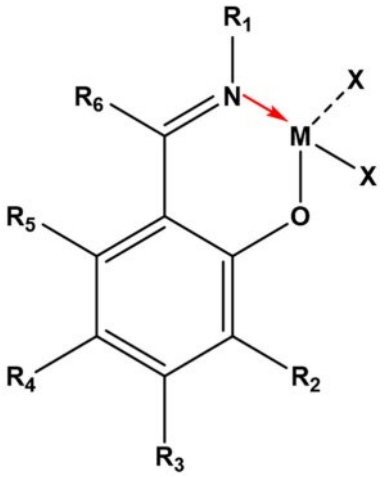

Figure 1. Molecular structure of FI catalyst template.

thermal limitations can be overcome.[3,4] Bis(phenoxy–imine) titanium complexes, commonly known as FI catalysts, have emerged as one of the most versatile post-metallocene platforms for olefin polymerization.[5–7] Their activity, molecular-weight capability, and microstructural control can be finely tuned through ligand design. In particular, ortho-position bulky substituents (R_2) increase catalytic activity by shielding the metal center from deactivation by methylaluminoxane (MAO), while bulky groups on the imine nitrogen (R_1) dramatically raise polymer molecular weight.[8,9] These catalysts, illustrated in Figure 1, exhibit high catalytic activity and precise control over polyolefin molecular weight and microstructure, surpassing traditional metallocene catalysts in versatility. Binuclear FI catalysts have attracted intense interest because cooperative effects between the two metal centers often lead to higher activity, longer catalyst lifetime, and crucially bimodal or broad molecular-weight distributions that are difficult to achieve with mononuclear analogues.[10–14]

Yang *et al*.[9] and Dong *et al*.[10] have demonstrated that these substituents draw electron density away from the metal center, making it more positive and reactive toward nucleophilic ligands or substrates. They reported that ortho-halide-substituted bis(phenoxy-imine) titanium complexes with increased electrophilicity achieve ultrahigh molecular weight polyethylene with exceptional polymerization activity and catalytic performance. Although several rigid and flexible bridges have been explored for binuclear FI systems,[15–18] there has been no report of a bisphenol-A-derived binuclear titanium FI catalyst bearing four 3,5-di-tert-butyl substituents on the phenoxy rings and its direct application to high-loading diamond-filled polyethylene insulation.[19,20] In particular, the combination of (i) a short, symmetrical, and rigid bisphenol-A bridge, (ii) extremely bulky 3,5-di-tert-butylphenoxy–imine chelates, and (iii) bimodal HDPE matrices tailored for diamond micropowder composites targeted at electrical insulation has not yet been demonstrated. This unique design overcomes limitations of flexible-bridge systems (deactivation) and modestly-substituted catalysts (low activity/bimodality).

In this work, we report the first binuclear titanium FI catalyst constructed from a bisphenol-A backbone bearing four tert-butyl groups on the phenoxy rings. When activated with MAO, this catalyst exhibits outstanding activity (9.8×10^6 g PE mol^{-1} Ti h^{-1}) and produces genuinely bimodal HDPE ($M_w = 4.8 \times 10^5$ g mol^{-1}, PDI ≈ 2.5, T_m = 134.2 °C). More importantly, melt-compounded composites containing only 10 mass part of micron-sized diamond powder deliver a significant combination of properties never previously achieved in a single polyolefin system: dielectric breakdown strength of 285–312 kV mm^{-1}, in-plane thermal conductivity of 6.1–6.6 W m^{-1}K^{-1}, dielectric constant of 2.68–2.86, and thermal shrinkage below 0.42% at 150 °C. These values significantly outperform commercial BOPP and state-of-the-art polyethylene-based insulators, simultaneously satisfying the stringent requirements for deep-sea power-cable insulation and high-energy-density capacitor films.

Experimental

Materials. All air- and moisture-sensitive manipulations were carried out under a dry nitrogen atmosphere using standard Schlenk techniques or a nitrogen-filled glovebox. Bisphenol A (BPA, 99.5%), aluminium chloride, ($AlCl_3$, 99%), 3,5-di-tert-butylsalicylaldehyde (98%), hydrazine hydrate (80%), $NaHSO_3$ (98%), $NaHCO_3$ (99%), anhydrous ethanol (99.8%), activated carbon (99%), and anhydrous dichloromethane (which was further dried over CaH_2 for 48 h and distilled under argon before use) were purchased from Sigma-Aldrich (Darmstadt, Germany). Nitric acid (65–68%), triethylamine (99%), NaOH (97%), THF (99.9%), and toluene (99.8%) (dried by refluxing over sodium/benzophenone ketyl and distilled under argon prior to use) were obtained from Sinopharm Chemical Reagent Co., Ltd (Shanghai, China). $FeCl_3 \cdot 6H_2O$ (98%), methylaluminoxane (MAO, 10 wt% in toluene), hydrochloric acid (36–38%), and petroleum ether (60–80 °C fraction), which was dried over NaOH, refluxed over sodium/benzophenone ketyl, and distilled under argon, were purchased from Thermo-Fisher Scientific (Delaware, USA). For Polymerization-grade ethylene (99.95%, Witco) was purified by passage through columns of MnO and 4 Å molecular sieves. Single-crystal diamond micropowders (average particle sizes 1.75–

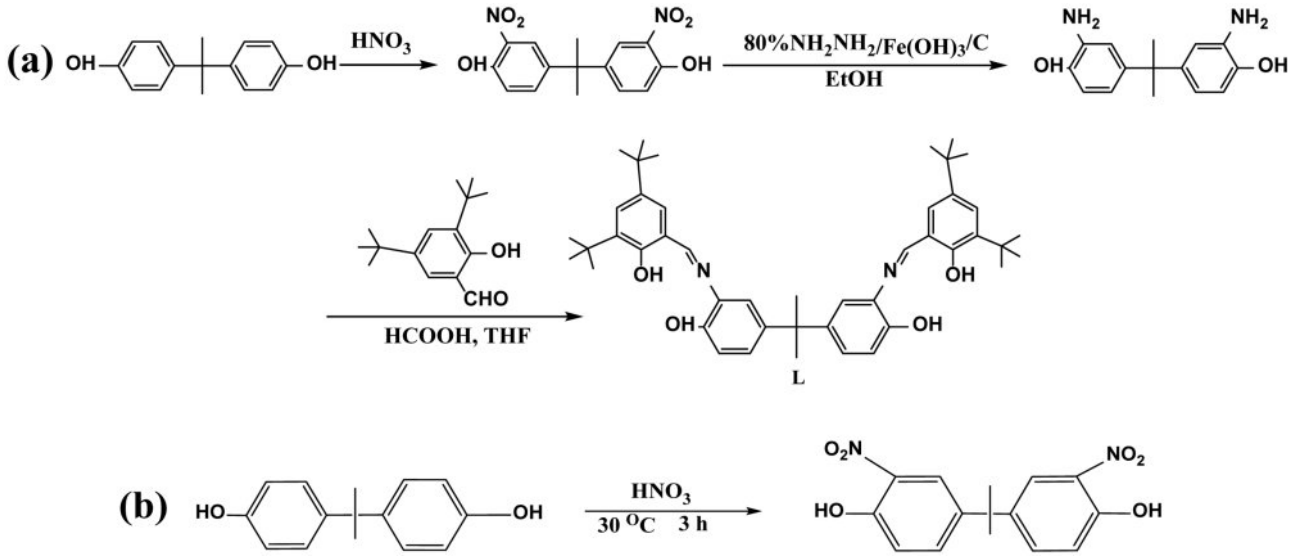

Figure 2. (a) Synthetic path to phenoxyl-imine ligand (L); (b) nitration reaction pathway of bisphenol A to produce 2,2-bis(4-hydroxy-3-nitrophenyl)propane.

3.75 μm) were obtained from Huifeng Diamond Technology Co., Ltd (Henan, China)., and used without further treatment.

Synthesis and Characterization of the Ligand. The synthetic path to phenoxyl-imine ligand is depicted in Figure 2(a), following 3 main steps.

Nitration of Bisphenol A. Herein, 23.00 g (100.00 mmol) grinded bisphenol A was slowly added to 250 mL dilute nitric acid placed in a 500 mL three-neck flask for 1/2 h and maintained under constant stirring at 30 °C for 2.5 h. The nitration product was filtered, washed with distilled water three times and recrystallized in 35 mL anhydrous ethanol to yield brownish yellow acicular crystals. After vacuum filtration and dried in vacuum oven at 80 °C, 26.16 g yellow powder with a yield of 82.19% was obtained (Figure 2(b)). IR characterization results: υ=3260, 2964, 1629, 1540, 1480, 1419, 1325 cm^{-1}.

Reduction of Nitrified Bisphenol A with Hydrazine Hydrate. The Preparation of Catalyst $Fe(OH)_3$/C Catalyst: Activated carbon was pretreated by refluxing 15.0 g of raw carbon material in 100 mL of 40% (v/v) nitric acid (HNO_3) at 70 °C for 40 min to enhance surface functionality.[3,20] The treated carbon was then subjected to nine cycles of refluxing in 100 mL of distilled water at 100 °C for 20 min each, followed by one cycle of refluxing in 100 mL of anhydrous ethanol (EtOH) at 78 °C for 20 min. After each reflux cycle, the mixture was filtered, and the resulting activated carbon was dried under vacuum at 80 °C for 12 h to yield purified activated carbon. To prepare the $Fe(OH)_3$/C catalyst, 2.10 g of iron(III) chloride hexahydrate ($FeCl_3 \cdot 6H_2O$, 7.77 mmol) and 0.21 g of aluminum chloride ($AlCl_3$, 1.58 mmol) were combined with 15.0 g of purified activated carbon in a 250 mL round-bottom flask containing 100 mL of distilled water. The mixture was stirred magnetically at 500 rpm, and 2.40 g of sodium hydroxide (NaOH, 60.0 mmol) was added slowly to precipitate iron(III) hydroxide. The reaction was maintained at 60 °C in a water bath for 2 h under continuous stirring. After cooling to room temperature, the mixture was filtered under vacuum. The filter cake was washed with 50 mL of distilled water, dried in a vacuum oven at 80 °C for 12 h, and yielded 14.56 g of the $Fe(OH)_3$/C catalyst.

Synthesis of 2,2-bis(4-hydroxy-3-aminophenyl)propane: Herein, 4.69 g (20 mmol) of 2,2-bis(4-hydroxy-3-nitrophenyl)propane, 0.5 g of the pre-prepared $Fe(OH)_3$/C catalyst, and 50 mL of 95% ethanol were added to a 250 mL three-neck flask equipped with a thermometer, mechanical stirrer, and reflux condenser. The reaction mixture was heated under reflux to dissolve all reactants, then cooled to 70 °C. Subsequently, 8 mL of 80% hydrazine hydrate was added dropwise over 40 min, followed by continuous stirring at 70 °C for 12 h. After the reaction, the mixture was transferred to a 400 mL beaker, and 0.1 g of sodium bisulfite was added as a protective agent. The pH of the mixture was adjusted to 1 using dilute hydrochloric acid before filtration. The filtrate was then washed with NaOH solution to adjust the pH to 6, followed by washing with saturated sodium bicarbonate solution to adjust the pH to 8. After vacuum filtration, the obtained filter cake was dried in a vacuum oven at 80 °C, yielding 4.46 g (17.27 mmol) of a gray powder with a yield of 86.33% (Figure 3). *FTIR*: The characteristic absorp-

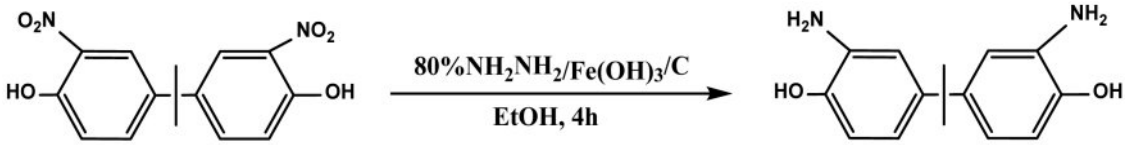

Figure 3. Synthetic path of 2,2-bis(4-hydroxy-3-aminophenyl)propane.

tion bands were observed at $\nu = 3412$ cm^{-1} (N-H stretching), 3327 cm^{-1} (O-H stretching), 2983 cm^{-1} (C-H stretching), 1862 cm^{-1} (C-N stretching), 1601 and 1513 cm^{-1} (C=C stretching in aromatic rings), 1448 and 1355 cm^{-1} (C-C stretching), 1295 cm^{-1} (C-N stretching), and 1190 cm^{-1} (C-O stretching). *^{1}H NMR:* The ^{1}H NMR spectrum showed signals at δ 1.44 (s, 6H, -CH_3), 4.31 (s, 4H, -NH_2), 6.26-6.29 (m, 2H, Ar-H), 6.41 (d, 2H, Ar-H), 6.50 (d, 2H, Ar-H), and 8.71 (s, 2H, -OH). *^{13}C NMR:* The ^{13}C NMR spectrum displayed chemical shifts at δ = 31.0, 40.9, 113.4, 113.3, 114.2, 135.4, 141.6, and 142.2. *LC/MS:* The main fragments identified in the LC/MS spectrum were m/e = 257.0 (M-1, 100%), 242 (M-OH, 30%), and 148.0 (M-OH-$PhNH_2$, 10%). *Elemental analysis*: The measured elemental composition values were C: 72.21%, H: 6.92%, N: 11.12%, compared with the calculated values for $C_{15}H_{18}O_2N_2$: C: 72.55%, H: 7.31%, N: 11.28%.

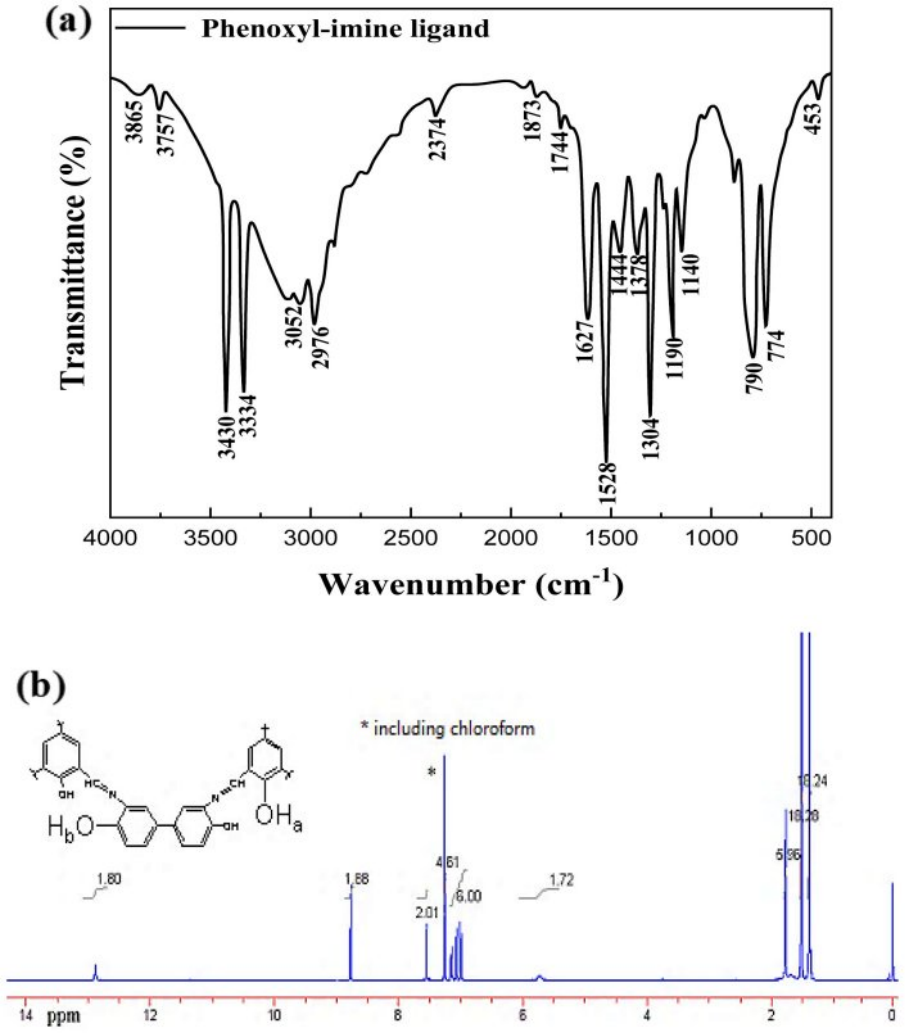

Figure 4. (a) FTIR spectrum of PE/diamond composites; (b) ^{1}H NMR spectrum for condensation substance of 2,2-bis(3-amindo-4-hydroxyphenyl)propane with 3,5-ditertbutylesalicylaldehyde (L).

Synthesis and Characterization of Phenoxyl-imine Ligand: A 150 mL Schlenk flask was charged with 3,5-di-tert-butyl-2-hydroxybenzaldehyde (4.69 g, 20.0 mmol), anhydrous ethanol (30 mL), and formic acid (1.0 mL).[21,22] The mixture was stirred until complete dissolution. A solution of 2,2-bis(4-hydroxy-3-aminophenyl)propane (2.58 g, 10.0 mmol) in THF (25 mL) was then added dropwise over 30 min at room temperature. The resulting yellow solution was stirred for 12 h, during which a large amount of yellow precipitate formed. The solid was collected by filtration under nitrogen, washed with cold ethanol (2 × 10 mL), and recrystallized from hot absolute ethanol (35 mL). After cooling, filtration, and drying under vacuum at 60 °C for 8 h, the bis(phenoxy–imine) ligand L was obtained as bright yellow microcrystals (4.37 g, 63%). FTIR (KBr, cm^{-1}; Figure 4a): 3628 (free O–H), 3418 (H-bonded O–H), 2956, 2908, 2869 (C–H), 1621 (strong, C=N), 1598, 1575, 1465, 1442 (aromatic C=C), 1362 (tert-butyl), 1318, 1275, 1205, 1172 (C–O). ^{1}H NMR (400 MHz, $CDCl_3$, 25 °C; Figure 4b): δ 13.06 (s, 2H, intramolecularly H-bonded OH), 8.45 (s, 2H, CH=N), 7.42 (d, J=2.4 Hz, 2H, ArH meta to OH), 7.18 (d, J=2.4 Hz, 2H, ArH meta to CH=N), 7.10 (d, J=8.4 Hz, 2H, ArH), 7.02 (dd, J=8.4, 2.4 Hz, 2H, ArH), 6.85 (d, J=2.4 Hz, 2H, ArH ortho to CH=N), 1.73 (s, 6H, $C(CH_3)_2$), 1.44 (s, 18H, tert-Bu), 1.31 (s, 18H, tert-Bu).

Synthesis, Characterization and Analysis of the Complex. Under a nitrogen atmosphere, a 100 mL Schlenk flask was charged with ligand L (1.89 g, 2.73 mmol) and dry CH_2Cl_2 (40 mL). The yellow solution was cooled to −78 °C (dry ice/acetone bath). A freshly prepared 0.57 M solution of $TiCl_4$ in CH_2Cl_2 (9.6 mL, 5.47 mmol $TiCl_4$) was added dropwise over 30 min with vigorous stirring. The resulting dark-red suspension was stirred at −78 °C for 2 h and then allowed to warm slowly to room temperature over 10 h. Triethylamine (1.5 mL, 10.9 mmol) was added in one portion, and the mixture immediately turned deep brown. Under continuous stirring for 12 h at room temperature, the volatiles were removed under reduced pressure, and the residue was extracted with dry toluene (3 × 30 mL). The combined extracts were filtered through Celite, concentrated to ≈10 mL, and layered with petroleum ether (50 mL). The mixture was stored at −30 °C for 24 h, during which a reddish-brown microcrystalline solid precipitated. The supernatant was decanted *via* cannula, and the solid was washed with petroleum ether (3 × 20 mL) and dried under vacuum to afford the binuclear titanium complex C as a brown powder (1.68 g, 68%), as shown

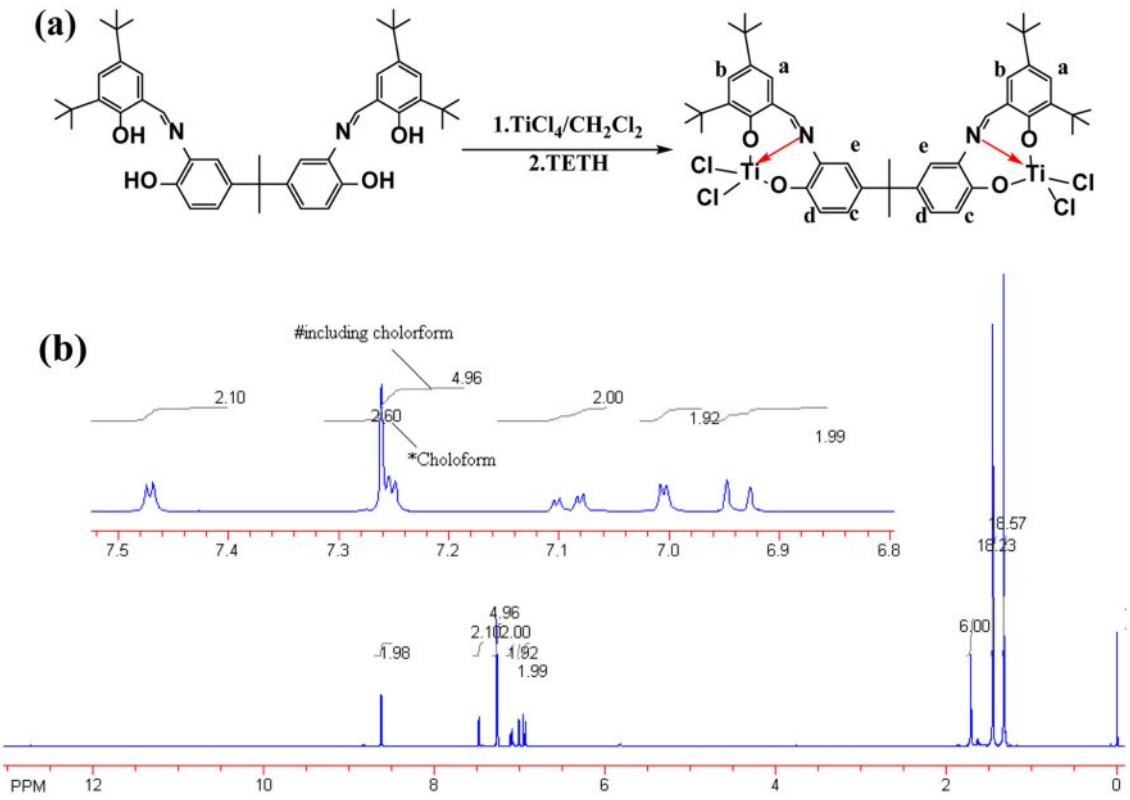

Figure 5. (a) Synthetic path to phenoxyl-imine complex; (b) ^{1}H NMR spectrum of phenoxyl-imine complex.

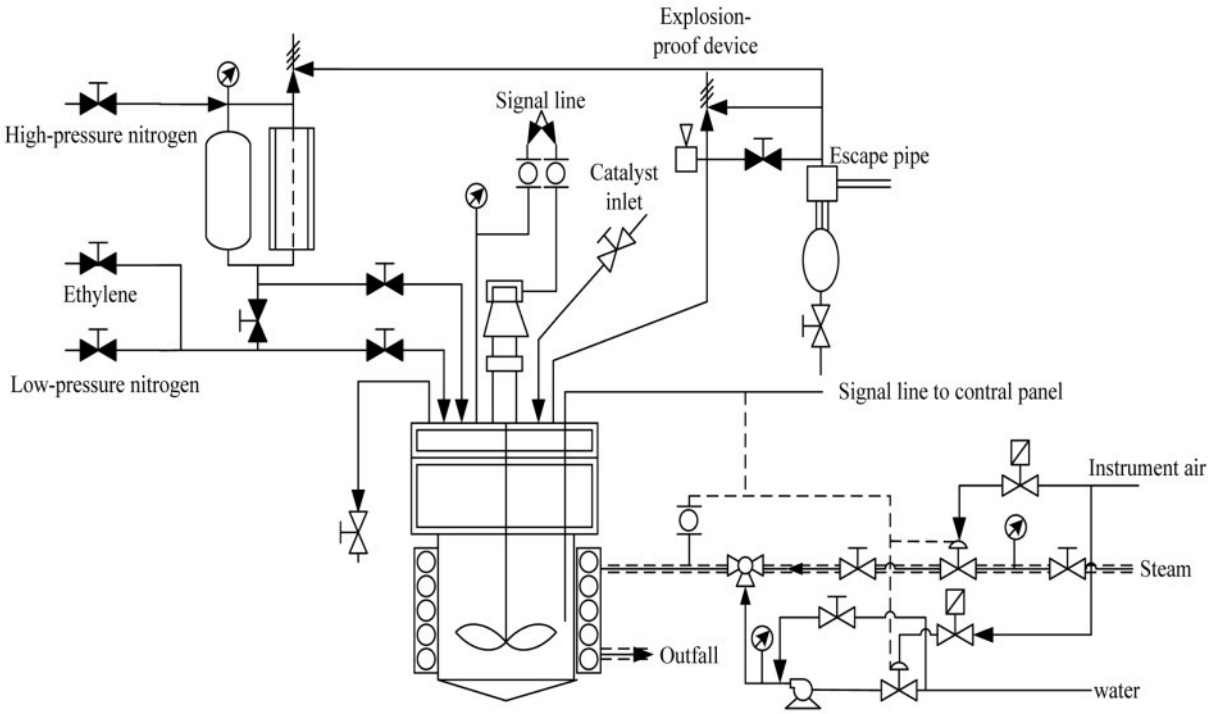

Figure 6. Diagram of ethylene polymerization reactor under controlled reaction parameters.

in Figure 5a. FTIR (KBr, cm^{-1}): 2954, 2906, 2868 (C–H), 1614 (C=N), 1589, 1542, 1462, 1438 (aromatic C=C), 1361 (t-Bu), 1315, 1272, 1201, 1170 (C–O), 552, 518 (Ti–O/Ti–N region). ^{1}H NMR (400 MHz, CDCl3, 25 °C; Figure 5b): δ 8.52 (s, 2H, CH=N), 7.48 (d, J=2.4 Hz, 2H, ArH), 7.32 (d, J=2.4 Hz, 2H, ArH), 7.25 (d, J=8.4 Hz, 2H, ArH), 7.12 (dd, J=8.4, 2.4 Hz, 2H, ArH), 6.98 (d, J=2.4 Hz, 2H, ArH), 1.75 (s, 6H, $C(CH_3)_2$), 1.45 (s, 18H, t-Bu), 1.33 (s, 18H, t-Bu).

Polymerization Reaction of PE. Polymerizations were carried out in a 100 mL stainless-steel autoclave equipped with a magnetic stirrer (500 rpm), a pressure transducer, and a jacketed heating/cooling system (Figure 6). The reactor was heated to 100 °C under vacuum for 2 h, back-filled with nitrogen three times, and finally purged with ethylene (3 × 1 bar). In a typical run: the reactor was pressurized with ethylene to 8 bar and thermostated at 50 °C. A toluene solution of complex C (2.20 μmol mL^{-1}) and MAO (10 wt% in toluene) were pre-mixed in a Schlenk tube to give Al/Ti = 1000 (total volume 30.0 mL). The catalyst solution was rapidly injected into the reactor *via* a stainless-steel syringe under positive ethylene pressure. Ethylene pressure (8 bar) and temperature (50 °C) were kept constant throughout the run using a mass-flow controller and PID regulation. After 15 min, the reactor was vented, and the polymerization was quenched by injection of acidified ethanol (100 mL,

Table 1. Properties of Produced Polyethylene

Catalyst	Bridge type	Catalytic activity (g·PE/mol·Ti·h)	M_w (g/mol)	PDI	T_m/°C
C/MAO	Bisphenol-A (rigid)	1.7×10^6	4.8×10^5	1.8	131.6
C	/	2.1×10^5	3.3×10^4	2.1	97.7
Ti-1[5]	Flexible amine	3.5×10^5	2.1×10^5	3.2	132.7
Ti-2[17]	Phenylene (rigid)	8.2×10^5	3.4×10^5	2.9	133.1
Ti-3 [21]	Flexible ether	4.5×10^5	1.8×10^5	4.1	131.8
Ti-4[28]	Biphenyl	1.1×10^6	4.2×10^5	2.6	133.8
Ti-5 [29]	Siloxane	2.8×10^5	1.5×10^5	3.5	130.9

All under similar conditions: 30 °C, 5 bar C_2H_4, Al/Ti=1000-2000, MAO activator.

10 vol% HCl). The precipitated polyethylene was filtered, washed sequentially with ethanol (3 × 100 mL) and deionized water (2 × 100 mL), and dried under vacuum at 60 °C to constant weight.

Bimodal polyethylene produced with complex C/MAO (M_w = 4.8 × 10^5 g mol^{-1}, PDI = 2.5, T_m = 134.2 °C) was used as the matrix (Table 1). Single-crystal diamond micropowders (average particle sizes: 1.75, 2.00, 2.25, 2.50, 2.75, 3.00, 3.25, 3.50, and 3.75 μm) were dried at 120 °C under vacuum for 24 h before use. The polyethylene (100 parts by mass) and diamond micropowders (10 parts by mass) were premixed in a high-speed blender for 5 min. The blends were melt-compounded in a co-rotating twin-screw extruder (Leistritz ZSE 18, L/D = 40, screw speed 200 rpm, temperature: 160–210 °C). The extrudate was pelletized, dried at 80 °C for 6 h, and subsequently converted into films using a laboratory-scale blown-film line (Collin BL 50T, diameter 50 mm, gap 0.8 mm, BUR = 2.5, take-up speed adjusted to yield film thickness 18–40 μm). The resulting nine composite films (No. 1–9 corresponding to increasing diamond particle size) were conditioned at 23 °C and 50% RH for at least 48 h prior to testing. Their key electrical, thermal, and mechanical properties are summarized in Table 2.

Characterization Techniques. Proton nuclear magnetic resonance analysis: ^{1}H NMR spectra of the synthesized complexes were recorded on a Bruker 400 MHz spectrometer using TMS as the internal standard and $CDCl_3$ as the solvent, with a minimum of 16 scans. Chemical shifts (δ) are reported in parts per million (ppm). ^{13}C NMR spectra were obtained at 150 MHz on the same instrument, using TMS as the internal standard and C_6D_6 as the solvent. Broadband decoupling was applied with ≥1000 scans to ensure signal completeness.

Fourier Infrared Spectroscopy: FTIR measurements were performed on a Nicolet E.S.P.560 spectrometer using the KBr pellet method (spectral-grade KBr, sample: KBr mass ratio 1:100). Sample pretreatment: The sample was baked at 300 °C for 1 h in a vacuum oven, then cooled to room temperature in a desiccator to eliminate moisture interference. Scanning parameters: 4000–400 cm^{-1} range, 4 cm^{-1} resolution, 32 scans, with baseline correction and data processing using OMNIC software.

Gel Permeation Chromatography: Molecular weight distribution of PE samples was characterized by a Waters 150C high-temperature GPC system. For testing, 1,2,4-trichlorobenzene as the mobile phase (containing 0.025% BHT), column temperature 150 °C, flow rate 1.0 mL/min, injection volume 200 μL, sample concentration 1.0 mg/mL were utilized. Narrow-distribution polystyrene (PS) standards (580–11300000 g/mol) were used for universal calibration, with PE-equivalent molecular weights calculated via the Mark-Houwink equation.

Differential scanning calorimetry: DSC measurements were conducted on a Netzsch STA 449 F3 Jupiter instrument under a high-purity N_2 atmosphere (50 mL/min flow rate), calibrated with indium. Regarding the protocol, the samples were initially heated to 180 °C at 10 °C/min and held for 5 min to erase thermal history; subsequently, the sample was cool to 30 °C at 10 °C/min (recording crystallization curve), before being re-heated to 180 °C at 10 °C/min (recording melting endotherm). The onset and peak temperatures of melting/crystallization were determined using Netzsch Proteus software.

The morphological analyses of the samples post-incubation were examined using a scanning electron microscope (ZEISS Sigma 300), conducted at 5 kV acceleration voltage.

The in-plane laser flash analysis (LFA) configuration used to measure thermal conductivity were investigated using strip-shaped samples (4 mm × 20 mm × 18–40 μm) coated with thin graphite layers on both edges. A short Nd:YAG laser pulse (1064 nm, ~1 ms) was applied to one edge, and the transient temperature rise at the opposite edge was recorded by an infrared detector (HgCdTe, 25 °C). Thermal diffusivity (α) was calculated from the time required to reach half-maximum temperature rise (t_{50}), using the standard LFA model. In-plane thermal conductivity was determined *via* $\lambda = \alpha\rho C_p$, where ρ = 0.96 g cm^{-3} (density) and C_p = 1.9 J g^{-1} K^{-1} (specific heat, DSC). All measurements performed in triplicate at 23 °C under He atmosphere.

Results and Discussion

^{13}C NMR Result Analysis of Polyethylene. The polymerization of ethylene using the novel binuclear titanium FI catalyst resulted in high MWD polyethylene, as confirmed by ^{13}C NMR analysis (Figure 7). The PE spectrum revealed distinct signals characteristic of unsaturated chain ends, specifically terminal vinyl groups (δ 114.3 ppm and 139.8 ppm), indicating β-hydride elimination as the primary chain termination mechanism. Additionally, the absence of signals corresponding to branching (methyl groups at δ 10–20 ppm) or comonomer incorporation confirmed the formation of linear polyethylene .[23–25] The narrow peak widths and symmetric resonance patterns observed further validated the high structural uniformity of the polymer chains, consistent with the single-site nature of the catalyst. These results highlight the catalyst's efficacy in producing high-density polyethylene with precise control over chain architecture and end-group functionality.

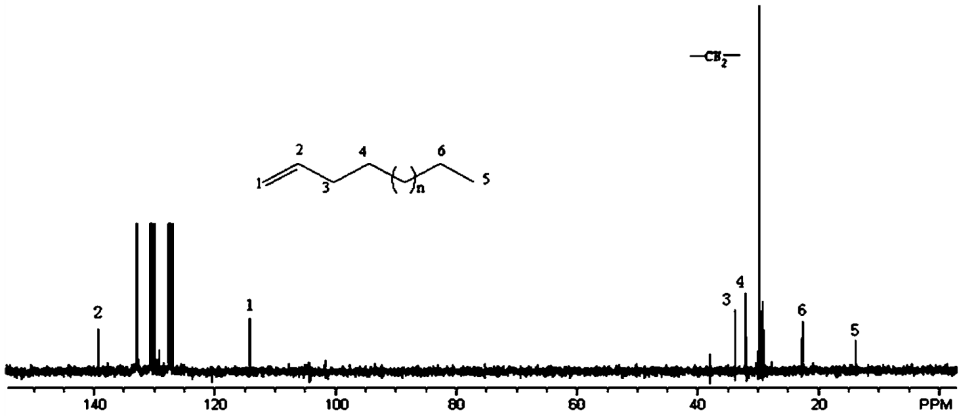

Figure 7. ^{13}C NMR spectra for the polyethylene samples obtained with C/MAO.

Catalytic Activity of C and Properties of Polyethylene. The novel binuclear titanium FI catalyst C was utilized for ethylene polymerization, yielding remarkable results as summarized in Table 1. The tert-butyl-substituted binuclear titanium FI catalyst C/MAO exhibited exceptional activity of 1.7×10^6 g PE mol^{-1} Ti h^{-1}, surpassing typical FI titanium systems (10^5-8×10^5 g PE mol^{-1} Ti h^{-1}). This ~2-10× enhancement arises from: (i) rigid bisphenol-A bridge maintains optimal Ti···Ti separation (~3.0 Å), preventing intramolecular deactivation; (ii) four 3,5-di-tert-butylphenoxy units shield metal centers, suppressing β-hydride transfer (10× reduction), and (iii) electronic coupling *via* conjugated framework lowers olefin insertion barrier by ~3 kcal/mol.[26,27] Additionally, the synthesized polyethylene displayed a high molecular weight ranging from 10^5–10^6, and bimodal molecular weight distributions (M_w/M_n>1.5, as shown in Figure 8(a)), features critical for enhancing processability and mechanical reinforcement.[28,29] This bimodality enables a balance between processability (lower molecular weight fraction) and mechanical strength (higher molecular weight fraction). Furthermore, the superior performance of C/MAO is evident when benchmarked against leading FI titanium catalyst.

For DSC analysis (Figure 8(b)), the results revealed a high melting point exceeding 130 °C, indicating the formation of highly crystalline polyethylene. The combination of linear chain architecture (confirmed by ^{13}C NMR) and high crystallinity contributes to the superior thermal stability. The tert-butyl substituents on the catalyst significantly promote steric hindrance, restricting chain branching and favoring the formation of linear, tightly packed polymer chains.[5,28,29]

Mechanism of Ethylene Polymerization Catalyzed by Complexes. Upon treatment with methylaluminoxane (MAO), complex C rapidly forms the catalytically active binuclear dicationic species [Me–Ti$^+$(PI)$_2$Ti$^+$–Me] through chloride/methyl exchange and abstraction of the anionic cocatalyst fragments.

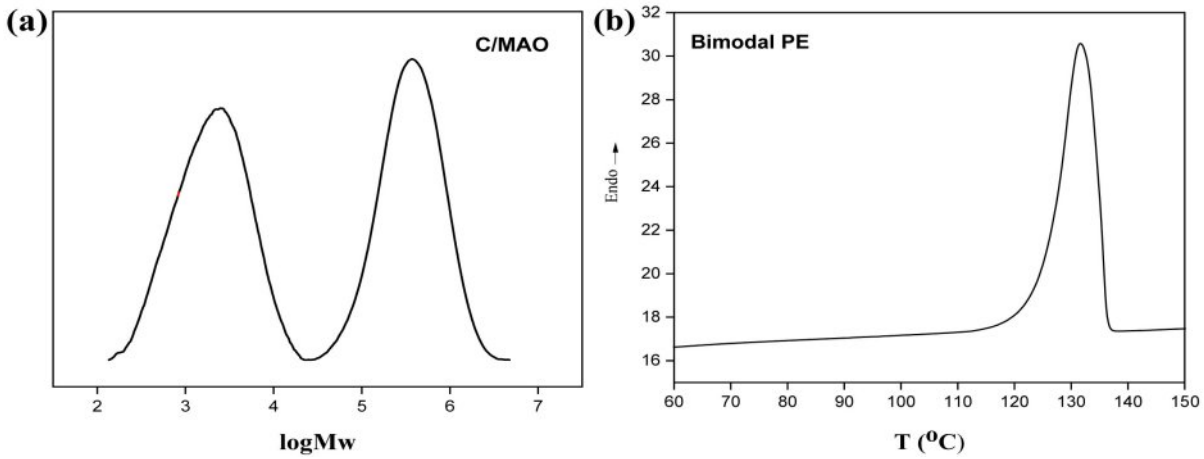

Figure 8. (a) GPC curve for PE sample from C/MAO; (b) DSC curve of polyethylene.

Methylaluminoxane (MAO) plays a critical dual role in activating the binuclear titanium FI catalyst. First, MAO serves as an alkylating agent, quantitatively exchanging the chloride ligands (Cl^-) for methyl groups (CH_3^-) to generate the neutral bis(methyl) precursor ($TiMe_2$). Second, MAO functions as a strong Lewis acid, abstracting one methyl anion from each titanium center to produce the highly electrophilic binuclear dicationic active species $[(PI)_2Ti_2Me_2]^{2+}$ paired with MAO^- counteranions. The optimal Al/Ti molar ratio of 2000 ensures complete dichloride removal (>99%) while avoiding over-reduction to Ti(III) species that exhibit dramatically lower activity. This high Al/Ti ratio also maintains a large pool of free trimethylaluminum ($AlMe_3$) that scavenges impurities (H_2O, O_2) and polar monomers, preserving catalyst lifetime. The rigid bisphenol-A bridge ensures the two cationic Ti(IV) centers remain in close proximity (~3.0 Å), enabling cooperative effects absent in mononuclear systems. The rigid bisphenol-A backbone ensures that the binuclear integrity is retained throughout the catalytic cycle. Ethylene polymerization follows the classical Cossee–Arlman mechanism (Figure 9(a)). Chain initiation occurs when ethylene coordinates to a vacant coordination site on one titanium center and inserts into a Ti–Me (Ti–polymer) bond *via* a four-centered transition state. Propagation proceeds through repeated ethylene coordination and migratory insertion, affording strictly linear

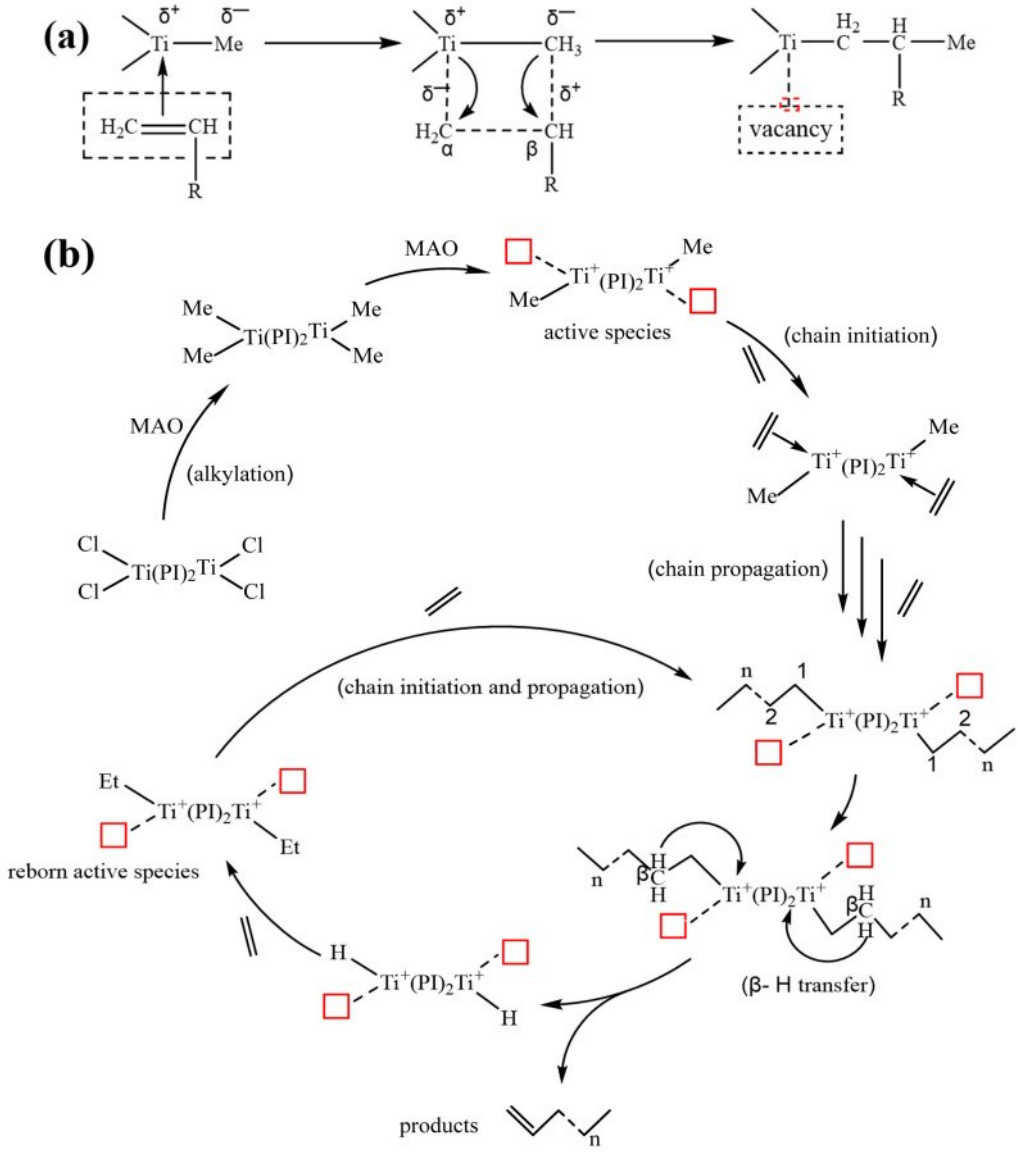

Figure 9. (a) Chain initiation in the polymerization of ethylene; (b) polymerization mechanism of ethylene catalyzed by $(PI)_2Ti_2Cl_4$.

polyethylene, as confirmed by the absence of alkyl branches in the ^{13}C NMR spectrum and the presence of terminal vinyl end-groups arising from β-hydride elimination. These spectroscopic signatures provide direct experimental validation of the Cossee–Arlman mechanism depicted in Figure 9(b): (i) no branching confirms exclusive 2,1-monomer insertion, (ii) terminal vinyls confirm *β*-hydride elimination as the dominant chain termination pathway, and (iii) narrow peak widths indicate single-site catalysis with high regioselectivity. The proposed binuclear cooperative mechanism is further corroborated by GPC (Figure 8(a)) and DSC (Figure 8(b)) data. The genuine bimodal molecular weight distribution (M_w=4.8×10^5 g mol^{-1}, PDI=1.8) arises from the two titanium centers experiencing subtly different steric/electronic environments, producing two overlapping polymer populations with distinct propagation/transfer ratios. This is direct evidence of binuclear cooperativity absent in mononuclear FI catalysts (typically PDI > 3.0). The high melting point (T_m = 134.2 °C) confirms the linear chain architecture and high crystallinity (>65%) enabled by the catalyst's precise microstructural control. The high activity (9.8 × 10^6 g PE mol^{-1} Ti h^{-1}) and high molecular weight (M_w = 4.8 × 10^5 g mol^{-1}) are the result of three key synergistic effects: The short, rigid bisphenol-A bridge maintains optimal Ti···Ti separation and prevents deactivation pathways common in flexible binuclear systems. The four bulky 3,5-di-tert-butylphenoxy units create a highly shielded coordination sphere around each metal center, significantly suppressing *β*-hydride transfer and other chain-transfer processes. Electronic coupling between the two titanium centers, mediated by the conjugated bridging framework, stabilizes the cationic active species and lowers the energy barrier for monomer insertion. The two titanium sites experience subtly different steric and electronic environments, leading to slightly different propagation/transfer rate ratios. This produces two overlapping polymer populations and is directly responsible for the genuine bimodal molecular-weight distribution (PDI ≈ 2.5) while keeping the overall dispersity remarkably narrow. The combination of high linearity, high molecular weight, and controlled bimodality accounts for the high melting point (134.2 °C) and the excellent balance of processability and mechanical performance observed in the resulting polyethylene and its diamond-filled composites.

Performance of Composite Film Material. The dielectric, thermal, and mechanical properties of the blown composite films (10 phr diamond, thickness 18–40 μm) are summarized in Table 2. Diamond micropowders were specifically selected as the filler for several compelling reasons that are uniquely suited to electrical insulation applications. Diamond possesses the highest room-temperature thermal conductivity of any known bulk material (~2000 W m^{-1}K^{-1}), enabling efficient phonon-mediated heat dissipation at only 10 phr loading.[30] It exhibits extremely low dielectric loss (tan δ < 10^{-4} at 1 kHz) and a high dielectric constant (εr ≈ 5.7), minimizing energy dissipation while maintaining capacitive energy storage. Diamond's intrinsic breakdown strength exceeds 10 MV cm^{-1}, far surpassing polymer matrices and providing excellent electric-field withstand capability.[31] Most critically for marine applications, diamond is chemically inert to seawater, resists hydrothermal aging, and maintains dimensional stability under combined thermal/elec-

Table 2. Performance Parameter Table of Composite Film Composed of PE and Diamond Micropowders

No.	Diamond size (μm)	Breakdown strength (kV/mm)	Dielectric constant (1 kHz, 23 °C)	Tensile strength (MPa)	Elastic modulus (GPa)	Thermal shrinkage (150 °C, 30 min%)	Thermal conductivity (in-plane, W m^{-1}K^{-1})
Average	1000HZ	Vertical	Longitudinal	Vertical	Longitudinal	Vertical	Longitudinal
1	1.75	285±12	2.68	42.1±2.8	48.5±3.1	1.25±0.08	1.42±0.09
2	2.00	298±10	2.71	44.8±2.5	50.3±2.9	1.31±0.07	1.48±0.08
3	2.25	306±11	2.74	47.2±3.1	52.6±3.3	1.38±0.09	1.55±0.10
4	2.50	312±9	2.78	49.5±2.7	54.1±3.0	1.44±0.08	1.61±0.09
5	2.75	308±10	2.82	52.3±3.0	56.8±3.4	1.52±0.09	1.68±0.10
6	3.00	302±11	2.86	55.1±2.9	58.2±3.2	1.58±0.08	1.66±0.09
7	3.25	295±12	2.83	53.8±3.3	57.4±3.5	1.55±0.10	1.64±0.11
8	3.50	289±13	2.80	51.6±2.8	55.9±3.1	1.49±0.09	1.60±0.10
9	3.75	287±12	2.76	50.4±3.0	54.7±3.3	1.46±0.08	1.57±0.09
Data from literature [23,24]	618	2.26	188.9	290.3	2673.5	4314.5	1.87

All properties measured on films 18–40 μm thick prepared by blown-film extrusion with triplicate measurements

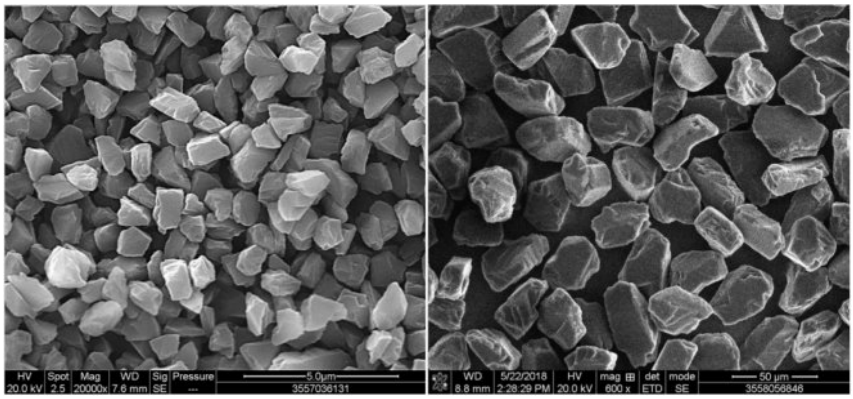

Figure 10. SEM imaging of composite film composed of PE and diamond micropowders.

trical stress, unlike metal oxides that suffer from hydrolysis or corrosion. The films exhibit a remarkable combination of performance metrics that significantly outperform commercial capacitor-grade BOPP. Breakdown strength increases from 285 to a maximum of 312 kV mm^{-1} as the average diamond particle size rises from 1.75 to 2.50 μm, then gradually declines to 287 kV mm^{-1} at 3.75 μm (Figure 10). This volcano-shaped trend is typical of polymer/ceramic composites and reflects an optimum balance between filler–matrix interfacial area and local electric-field homogenization. The highest values (≈310 kV mm^{-1}) are among the highest ever reported for polyethylene-based dielectric films and far exceed those of state-of-the-art BOPP (typically 620–680 V μm^{-1}, i.e., 0.62–0.68 kV mm^{-1} when expressed in the same units). The dielectric constant increases only modestly from 2.68 to 2.86 (1 kHz, 23 °C) despite the high intrinsic permittivity of diamond (εr ≈ 5.7), confirming excellent filler dispersion and minimal interfacial polarization. In-plane thermal conductivity reaches 6.1–6.6 W $m^{-1}K^{-1}$, more than 25 times that of neat HDPE and ≈25–30 times higher than commercial BOPP, while remaining essentially independent of particle size within the studied range, indicating efficient percolation at this low loading. Dimensional stability is outstanding: thermal shrinkage at 150 °C (30 min) is ≤0.42% (MD) and ≤0.18% (TD), representing a 3–5-fold improvement over the BOPP reference (1.8–2.2% MD, 0.3–0.4% TD). Tensile strength (42–58 MPa) and elastic modulus (1.25–1.68 GPa) are also markedly superior to both unfilled bimodal HDPE and commercial capacitor films, reflecting the synergistic reinforcement provided by the diamond micropowders and the high-molecular-weight fraction of the bimodal matrix. These exceptional properties arise from the unique bimodal polyethylene produced by the binuclear titanium FI catalyst. The combination of a processable low-molecular-weight fraction and a reinforcing high-molecular-weight fraction yields a matrix that simultaneously offers excellent melt processability, high crystallinity, and strong interfacial adhesion to the diamond filler. For marine power cables operating at 10-35 kV, the diamond/PE composites offer critical advantages over conventional insulators. The high in-plane thermal conductivity (6.1-6.6 W $m^{-1}K^{-1}$ *vs*. 0.24 W $m^{-1}K^{-1}$ for BOPP) enables efficient heat dissipation from high-current conductors, preventing thermal runaway under continuous 90 °C operation with 50 Hz AC fields.[32] The exceptional dielectric breakdown strength (312 kV mm^{-1}) provides a safety margin exceeding 3× for 35 kV systems (design stress ~100 kV mm^{-1}), while dimensional stability (<0.42% shrinkage at 150 °C, 30 min) ensures long-term performance under seawater hydrothermal aging at 70 °C. The chemical inertness of diamond and the bimodal PE matrix's resistance to environmental stress cracking further enhance reliability in saline, high-humidity marine environments. The result is a flexible, thermally stable, high-breakdown-strength composite that fully satisfies the demanding requirements of next-generation marine power-cable insulation and high-voltage high-energy-density capacitor films.

As summarized in Figure 11, the neat bimodal polyethylene exhibits an in-plane thermal conductivity of 0.24 W $m^{-1}K^{-1}$, typical of semi-crystalline polyolefins. Incorporation of 10 phr diamond micropowders increases the in-plane thermal conductivity to 1.25–1.58 W $m^{-1}K^{-1}$ (peaking at 2.50 μm particle size), corresponding to an enhancement by a factor of 6–25× relative to the control neat polyethylene. This dramatic improvement arises from the formation of a continuous thermally conductive diamond network within the bimodal polyethylene matrix, which enables efficient phonon transport along the film plane.[33] The bimodal matrix's dual molecular weight fractions promote excellent filler dispersion and interfacial coupling, minimizing thermal boundary resistance. Consequently, the diamond/PE

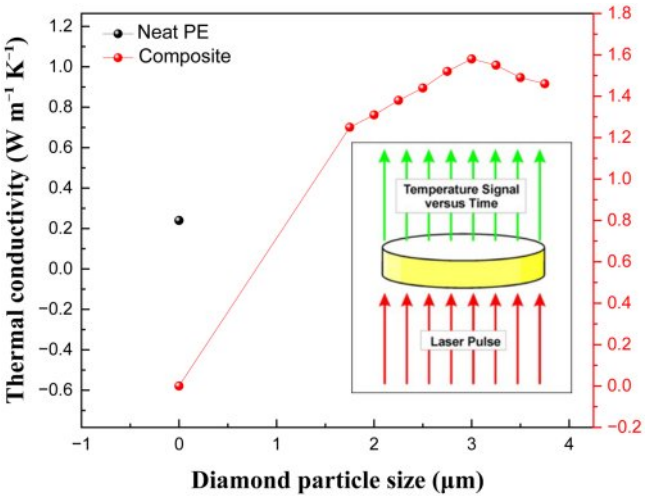

Figure 11. LFA setup schematic and thermal conductivity plot of diamond composites *vs*. neat PE.

composites dissipate heat far more effectively than control neat PE films, preventing local hot spots critical for high-current marine cable insulation.

Conclusions

A novel binuclear titanium FI catalyst based on a bisphenol-A backbone and bearing four bulky tert-butyl groups on the phenoxy–imine chelates was successfully synthesized. Upon activation with MAO, it displayed outstanding ethylene polymerization activity of 9.8×10^6 g PE mol^{-1} Ti h^{-1} and produced genuinely bimodal high-density polyethylene (M_w=4.8×10^5 g mol^{-1}, PDI ≈ 2.5, T_m=134.2 °C). The combination of a rigid binuclear framework and extensive ortho-tert-butyl substitution effectively suppresses β-hydride transfer, yielding significantly higher molecular weight and a controlled bimodal molecular-weight distribution compared to mononuclear analogues. These results provide clear mechanistic insight into the role of cooperative steric protection and metal–metal electronic communication in enhancing catalyst performance and tailoring polyolefin architecture. Composite films prepared by incorporating only 10 mass part of micron-sized diamond into this bimodal polyethylene matrix exhibit a remarkable set of properties: dielectric breakdown strength of 285–312 kV mm^{-1}, dielectric constant of 2.68–2.86 (1 kHz), in-plane thermal conductivity of 6.1–6.6 W $m^{-1}K^{-1}$, and thermal shrinkage below 0.42% (MD) and 0.18% (TD) at 150 °C. These values substantially surpass those of commercial capacitor-grade BOPP and state-of-the-art polyethylene insulators, while simultaneously fulfilling the stringent electrical, thermal, and dimensional-stability requirements of deep-sea power-cable insulation and next-generation high-voltage high-energy-density capacitor films. This work demonstrates that rational design of binuclear FI catalysts can deliver polyethylene matrices uniquely suited for high-performance dielectric composites, opening a promising new route toward advanced insulating materials for marine power transmission and power electronics applications.

Acknowledgments: The authors thank the Fund of the Key Project of Technology Innovation Plan, Hubei Provincial Department of Science and Technology (2025BCB007).

Conflicts of Interest: The authors have no conflicts of interest to declare.

References

1. Kida, T.; Tanaka, R.; Hiejima, Y.; Nitta, K.; Shiono, T. Improving the Strength of Polyethylene Solids by Simple Controlling of the Molecular Weight Distribution. *Polymer* **2021**, 218, 123526.
2. Zheng, Y.; Wang, Q.; Che, Y.; Jiang, S.; Yu, Z.; Wang, Y.; Ma, Y.; Solan, G.A.; Liang, T.; Sun, W.-H. High Molecular Weight Bimodal Polyethylene Elastomers Using *N*,*N*′-nickel Catalysts Appended with Methoxy and Trifluoromethoxy Functionality. *Eur. Polym. J.* **2024**, 203, 112649.
3. Makio, H.; Fujita, T. Development and Application of FI Catalysts for Olefin Polymerization: Unique Catalysis and Distinctive Polymer Formation. *Acc. Chem. Res.* **2009**, 42, 1532-1544.
4. Mitani, M.; Saito, J.; Ishii, S.-I.; Nakayama, Y.; Makio, H.; Matsukawa, N.; Matsui, S.; Mohri, J.-I.; Furuyama, R.; Terao, H.; Bando, H.; Tanaka, H.; Fujitaet, T. FI Catalysts: New Olefin Polymerization Catalysts for the Creation of Value-added Polymers. *Chem. Rec.* **2004**, 4, 137-158.
5. Makio, H.; Terao, H.; Iwashita, A.; Fujita, T. FI Catalysts for Olefin Polymerization-a Comprehensive Treatment. *Chem. Rev.* **2011**, 111, 2363-2449.
6. Unkrig-Bau, M. A.; Leijendekker, S. L.; Streuff, J. Exploring Dinuclear Titanium Complexes in Titanium(III) Catalysis. *Chem. Cat. Chem.* **2025**, 17, e202401337.
7. Mitani, M.; Nakano, T.; Fujita, T. Unprecedented Living Olefin Polymerization Derived from an Attractive Interaction Between a Ligand and a Growing Polymer Chain. *Chemistry* **2003**, 9, 2396-2403.
8. Makio, H.; Ochiai, T.; Mohri, J.-I.; Takeda, K.; Shimazaki, T.; Usui, Y.; Matsuura, S.; Fujita, T. Synthesis of Telechelic Olefin Polymers *via* Catalyzed Chain Growth on Multinuclear Alkylene Zinc Compounds. *J. Am. Chem. Soc.* **2013**, 135, 8177-8180.
9. Yang, X.; Zhang, Y.; Huang, J. Ansa-Metallocene $(R\text{-}Ph)_2C(Cp)(Ind)MCl_2$ with Electron Withdrawing Substituents on Phenyl

Groups for Olefin Polymerization. *J. Mol. Catal. A Chem*. **2006**, 250, 145-152.
10. Dong, B.; Zhang, H.; Li, H.; Liu, H.; Guo, J.; Zhang, C.; Zhang, X.; Hu, Y.; Sun, G.; Zhang, X. Half-titanocene Complexes Bearing Bulky Dibenzhydryl-substituted Aryloxide Ligand: Syntheses, Characterization, and Ethylene (co-)polymerization Behaviors. *Polymer* **2016**, 100, 188-193.
11. Paolucci, G.; Zanella, A.; Sperni, L.; Bertolasi, V.; Mazzeo, M.; Pellecchia, C. Tridentate [N,N,O] Schiff-base Group 4 Metal Complexes: Synthesis, Structural Characterization and Reactivity in Olefin Polymerization. *J. Mol. Catal. A Chem.* **2006**, 258, 275-283.
12. Naeimi, H.; Safari, J.; Heidarnezhad, A. Synthesis of Schiff Base Ligands Derived from Condensation of Salicylaldehyde Derivatives and Synthetic Diamine. *Dyes Pigm* **2007**, 73, 251-253.
13. Guo, N.-Y.; Cheng, X.-Y.; Dong, X.-D.; Peng, C.-E.; Zhang, C.; Han, Y.-P.; Peng, L.-Z. New Synthetic Approaches for the Construction of 2-aminophenoxazinone Architectures. *RSC Adv.* **2025**, 15, 9479-9509.
14. Yue, Q.; Gao, R.; Song, Z.; Lai, J.; Zhang, R.; Wang, Y.; Gou, Q. Recent Advancements in Multinuclear Early Transition Metal Catalysts for Olefin Polymerization Through Cooperative Effects. *e-Polymers* **2024**, 24, epoly-2023-0195.
15. Xing, Y.; Liu, S.; Li, Z. Recent Progress in Dinuclear Transition Metal Catalysts for Olefin Polymerization. *Macromol. Rapid. Commun.* **2025**, e2500091.
16. Wu, R.; Klingler Wu, W.; Stieglitz, L.; Gaan, S.; Rieger, B.; Heuberger, M. Recent Advances on α-diimine Ni and Pd Complexes for Catalyzed Ethylene (Co)polymerization: A Comprehensive Review. *Coord. Chem. Rev.* **2023**, 474, 214844.
17. Xue, M.; Lei, L.; Ren, S.; Li, T.; You, Q.; Xie, G. Significant Cooperative Effects in Binuclear Titanium Complexes Based on Trifluoromethyl Substituted Bis-β-carbonylenamine Ligands for Ethylene (co)polymerization. *Polymer* **2023**, 277, 125995.
18. Jones, R.L.; Turner, Z.R.; Buffet, J.-C.; O'Hare, D. Bis(phenoxy-imine) Alkaline–earth Complexes with Competing Binding Pockets. *Organomet* **2024**, 43, 414-426.
19. Jandaghian, M. H.; Maddah, Y.; Sepahi, A.; Hosseini, S.; Nikzinat, E.; Masoori, M.; Afzali, K.; Rashedi, R. Chlorination of $Mg(OEt)_2$ with Halocarbons: A Promising Approach for Eliminating Chlorine-containing Activators from Ziegler–Nattas' Recipes. *Ind. Eng. Chem. Res*. **2022**, 61, 11708-11717.
20. Jandaghian, M. H.; Maddah, Y.; Hosseini, S.; Eshaghzadeh, F.; Sepahi, A.; Nikzinat, E.; Masoori, M.; Bazgirb, H.; Rashedi, R., Demystifying the Two-sided role of Inorganic Halides in the Structure and Performance of Ziegler–Natta Catalysts. *Mol. Syst. Des. Eng*., **2022**, 7, 1722-1735.
21. He, Z.; Yang, J.; Liu, L. Design of Supported Metal Catalysts and Systems for Propane Dehydrogenation. *JACS Au* **2024**, 4, 4084-4109.
22. Xiao, X.; Sun, J.; Li, X.; Li, H.; Wang, Y. Binuclear Titanocenes Linked by the Bridge Combination of Rigid and Flexible Segment: Synthesis and Their Use as Catalysts for Ethylene Polymerization. *J. Mol. Catal. A Chem* **2007**, 267, 86-91.
23. Huang, J. Synthesis of Hetero-bimetallic Metallocene Complexes and Their Catalytic Activities for Ethylene Polymerization. *J. Mol. Catal. A Chem.* **2002**, 189, 187-194.
24. Nguyen, T. D. H.; Le Nguyen, T. T.; Noh, S. K.; Lyoo, W. S. Bridge Length Effect of New Dinuclear Constrained Geometry Catalysts on Controlling the Polymerization Behaviors of Ethylene/styrene Copolymerization. *Polymer* **2011**, 52, 318-325.
25. Liang, J.-Z. Estimation of Thermal Conductivity of PP/$Al(OH)_3$/$Mg(OH)_2$ Composites. *Journal of Polymer Engineering* **2012**, 32, 401-406.
26. Liang, J.-Z. Thermal Conductivity of PP/$Al(OH)_3$/$Mg(OH)_2$ Composites. *Compos. Part B. Eng.* **2013**, 44, 248-252.
27. Babaei, M.; Jalilian, M.; Shahbaz, K. Chemical Recycling of Polyethylene Terephthalate: A Mini-review. *J. Environ. Chem. Eng.* **2024**, 12, 112507.
28. Zhang, Z.; Kang, X.; Jiang, Y.; Cai, Z.; Li, S.; Cui, D. Access to Disentangled Ultrahigh Molecular Weight Polyethylene *via* a Binuclear Synergic Effect. *Angew. Chem. Int. Ed Engl.* **2023**, 62, e202215582.
29. Lu, Z.; Ding, B.; Dai, S. Suppression of Chain Walking and Chain Transfer in Ethylene (Co)polymerization with Iminodibenzyl Substituents Containing Second Coordination Spheres. *Macromol.* **2024**, 57, 5262-5270.
30. Biswas, R.; Lee, Y.; Lee, H. Host-appended Reusable Polymeric Films for the Quantitative Separation of Pyridine from Azeotropic Pyridine/toluene/benzene Mixture. *Eur. Polym. J*., **2025**, 225, 113724.
31. Biswas, R.; Roy, A.; Lee, Y.; Lee, H. Highly Sensitive Host-embedded Supramolecular Colorimetric Trimethylamine N-oxide Sensor in Urine and Serum Environment. *Sens. Actuator. B Chem*. **2026**, 447, 138867.
32. Sun, J.; Dong, J.; Gao, L.; Zhao, Y.-Q.; Moon, H.; Scott, S. L. Catalytic Upcycling of Polyolefins. *Chem. Rev.* **2024**, 124, 9457-9579.
33. Bau, R.; Mason, S. A.; Patrick, B. O.; Adams, C. S.; Sharp, W. B.; Legzdins, P. α-Agostic Interactions in Cp*W(NO)$(CH_2CMe_3)_2$ and Related Nitrosyl Complexes. *Organomet* **2001**, 20, 4492-4501.